International Journal of Hydrological and Environmental for Sustainability
Volume 1, Issue 1, 08-23
e_ISSN: 2828-5050
https://www.journal.foundae.com/index.php/ijhes

Geophysical Analysis Using Proton Precession Magnetometer GSM-19T as Information on Fault Presence in Medana, North Lombok, Indonesia

Haerul Anwar*
Department of Environmental Engineering,
Institut Kesehatan dan Teknologi PKP DKI Jakarta,
INDONESIA

Vico Luthfi Ipmawan
Department of Physics,
Institut Teknologi Sumatera,
INDONESIA

Thanaporn Sriyakul
Department of Management,
Mahanakorn University of Technology
THAILAND

***Correspondence: E-mail:** anwar.haerul90@gmail.com

Article Info

Article history:

Received: December 31, 2021
Revised: February 04, 2022
Accepted: February 06, 2022

Abstract

Lombok island is included in one of the areas prone to earthquakes due to the existence of a subduction zone resulting from the meeting of the Indian-Australian Plate. In this study, the magnetic method was used to determine the subsurface structure of the fault as a research objective. The instrument used in this study consisted of a Proton Precession Magnetometer GSM-19T v7.0 Geomagnet measuring instrument with an accuracy of 0.1 nT to measure the total magnetic field strength. Garmin 60CSx GPS to determine position (latitude and longitude), elevation, time and point of measurement location. The geological compass determines the position and direction of the north-south fault which includes the dip/strike. Some software is also used in processing this geomagnetic data, namely Software (Numeri, Mag2DC, Surfer 9.0) and MS Excel 2013. Based on the results of data processing with 2D and Mag2DC forward modeling, the subsurface structure is obtained in the form of a normal fault, with the average susceptibility value is 0.00605 in Susceptibility (SI) which is a type of limestone. The depth of this normal fault is estimated to be at a depth of 31.5 meters to 74.0 meters.

Keywords: geophysical analysis; fault; PPM geomagnet; Mag2DC; surfer 9.0

To cite this article: Anwar, H., Ipmawan, V, L. and Sriyakul, T. (2022). Geophysical Analysis Using Proton Precession Magnetometer GSM-19T as Information on Fault Presence in Medana, North Lombok, Indonesia. *International Journal of Hydrological and Environmental for Sustainability, 1*(1), 08-23. https://doi.org/10.58524/ijhes.v1i1.57

INTRODUCTION

Indonesia is an archipelagic country located at the confluence of three of the world's active tectonic plates, namely the Eurasian Plate which moves from the north, the Indian–Australian Plate from the south, plus the movement of the Pacific Plate from the east. The movement of these plates can be in the form of subduction (upward plate movement), obduction (downward plate movement) and collision (plate collision) and divergence (plate collision) (Watlet et al., 2020). The movement of these plates causes the territory of Indonesia to have a unique and complex geological arrangement, so that the Indonesian territory is tectonically a very active and unstable area that is prone to earthquakes at all times (Taruna & Banyunegoro, 2018). The meeting of the Indian–Australian Plate with the Eurasian Plate along the Indonesian archipelago forms the Sunda Arc, which starts from the island of Sumatra and ends in the Nusa Tenggara Islands. This arc is one of the areas with a high frequency of earthquakes (Meijaard et al., 2019).

Lombok Island is one of the areas prone to earthquakes. This is due to the presence of a subduction zone resulting from the meeting of the Indian-Australian Plate with the Eurasian Plate in the south of Lombok Island and the active Flores thrust fault formed by the subduction of the Eurasian Plate against the Indian-Australian Plate in the north (Thoreau, 2010). This plate movement

is the trigger for the activation of the faults that cross most areas of the island of Lombok. If these faults become active, the area they pass through becomes prone to earthquakes (Haerudin et al., 2019). For areas with these characteristics, the distribution of earthquakes that occur is generally shallow, which is less than 30 km **(Figure 1)**.

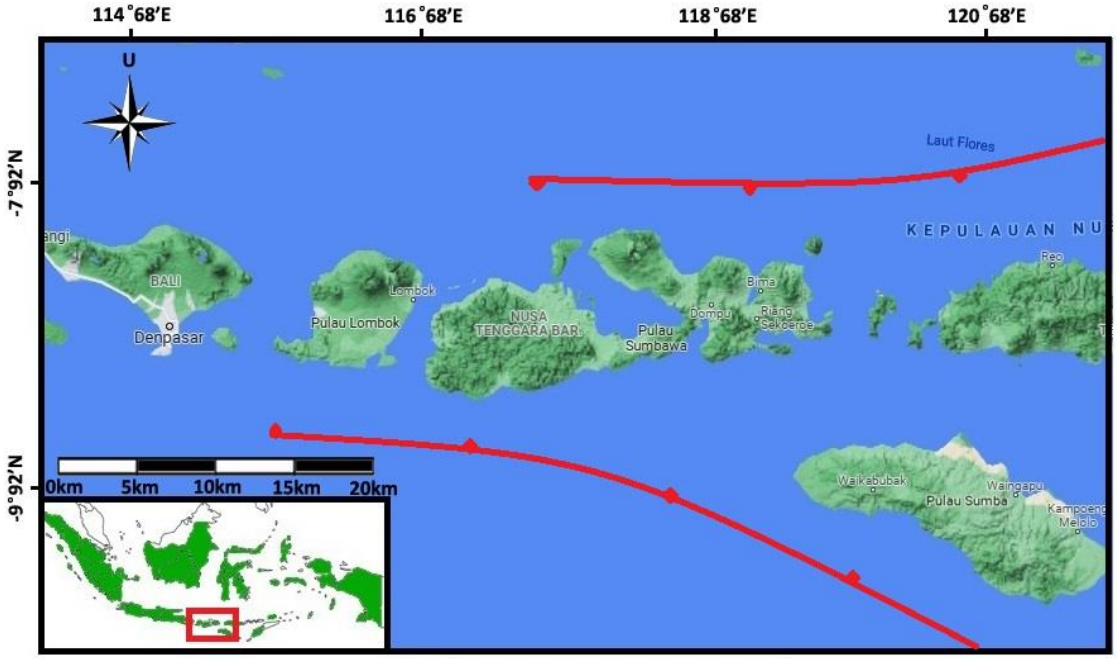

Figure 1. Geographical conditions of the Lombok island, Indonesia

The existence of faults on the island of Lombok so far has received low attention, this can be seen from the lack of research related to the existence of these faults, so that so far there is no certainty about their existence (Ashok & Umamahesh, 2019; Peker et al., 2024; Weihua et al., 2012). One of the fault predictions on the island of Lombok crosses North Lombok Regency which is located in the southern part of Tanjung District. The existence of this fault is very important because it has a history of quite high seismicity, recorded since 1979 – 2007 with coordinates 70 South Latitude – 120 South Latitude and 1150 East Longitude – 1160 East Longitude, at least 22 earthquakes have occurred with a magnitude scale 5 SR (Source: NEIC-USGS). Finally, on June 22, 2013 an earthquake measuring 5.4 on the Richter scale occurred in North Lombok Regency, with its center on land with coordinates 8.43 South Latitude – 116.04 East Longitude, 14 km northwest of West Lombok at a depth of 10 km. One of the areas that suffered severe physical damage due to the earthquake was Medana Village, Tanjung District. A total of 342 buildings were badly damaged, 79 buildings were moderately damaged, and 174 buildings were slightly damaged (Haseeb et al., 2011; Mahla, 2018; Sherpa, 2010; Wekke et al., 2019).

Determination of faults can be done by geophysical surveys, where in geophysical surveys there are many methods that can be used to determine faults, one of which is the geomagnetic method. This method is based on measuring variations in magnetic intensity on the earth's surface caused by variations in the distribution (anomalies) of magnetized objects below the earth's surface. Magnetic anomaly occurs because of the variation of the magnetic field towards the spatial towards the regional (Diani et al., 2019). This anomalous pattern is characterized by alternation between positive-negative anomalies and parallel to the pemekeran axis.

Faults in a rock can be likened to imagining a magnet being split into two parts. If there is no physical change in the rock or a change in position at the fault event, then this will not cause anomalous changes. However, if there is a change in the physical properties of the rock, such as a rock metaformation event or an increase in the layer due to pressure from the layer, there will be a change in magnetic anomaly. Changes in magnetic anomaly can also occur due to the presence of rock filling fractures, where the rock is mineral rock or lava instructions. If the fracture is filled with lava-instructed rock, it will cause an anomalous jump (Maryanto, 2017; Thoreau, 2010).

In this study, a magnetic method was used to determine the subsurface structure of the fault. This method was chosen because in addition to utilizing the magnetic properties of rocks without damaging the subsurface structure of the study area, also because it has a fairly high measurement accuracy, instrumentation and operation in the field are relatively simple, easy and fast when compared to other geophysical methods and are environmentally friendly. This method is very suitable for preliminary surveys with a fairly wide area coverage.

METHOD

The methodology describes in detail the steps taken in this study. The explanation of these steps starts from the preparation stage, field activities to field data analysis and then ends with results that are in accordance with the research objectives. In data collection, the number of people as volunteers who helped as many as 15 people.

Research Location and Time

This research was conducted in Medana Village, Tanjung District, North Lombok Regency, West Nusa Tenggara Province. The research location is shown in **Figure 2**. This research was carried out from July 2020 to December 2020. Data collection was carried out on July 21, 2020 in three hamlets, namely Orong Rumput Hamlet, Kopang Hamlet and Gol Hamlet, Medana Village, Tanjung District, North Lombok Regency, West Nusa Tenggara Province.

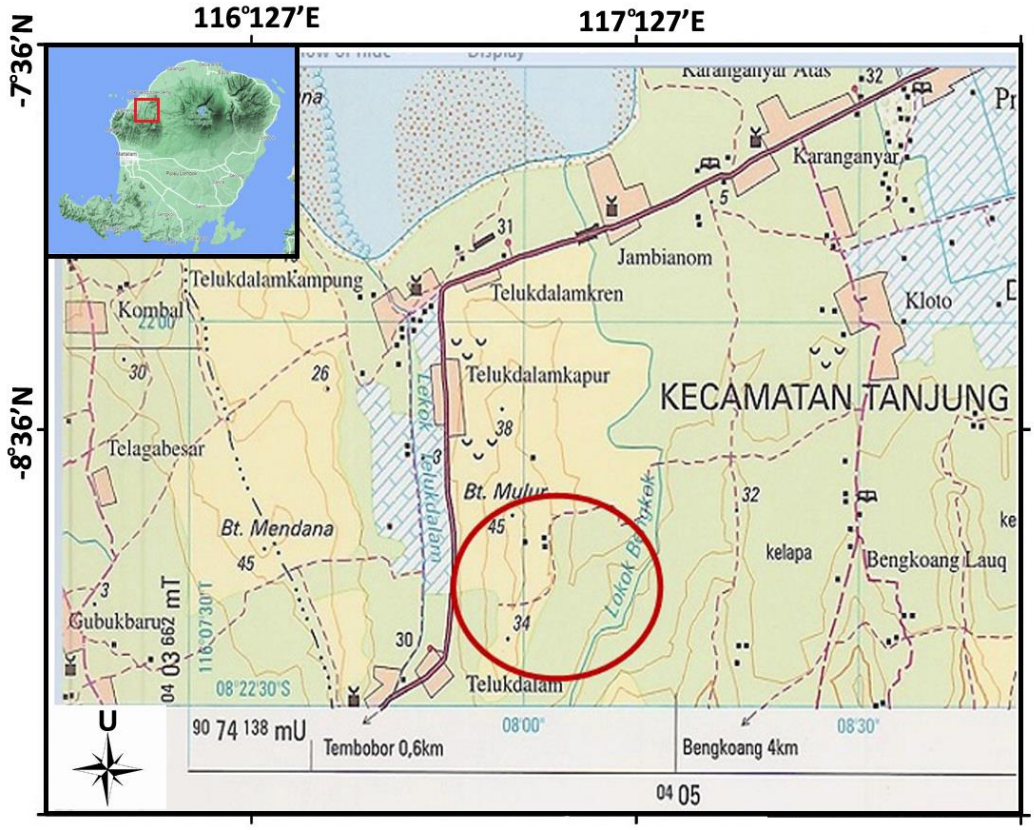

Figure 2. Research site map

Research Equipment

The instrument used in this study consisted of a Proton Precision Magnetometer GSM-19T v7.0 Geomagnet measuring instrument with an accuracy of 0.1 nT to measure the total magnetic field strength. Garmin 60CSx GPS to determine position (latitude and longitude), elevation, time and point of measurement location. The Geological Compass determines the position and direction of the north-south fault which includes the dip/strike. Some software is also used in processing this geomagnetic data, namely Software (Numeri, Mag2DC, Surfer 9.0) and MS Excel 2013.

Data Acquisition

Before carrying out geomagnetic data acquisition, first determine the measurement trajectory. In this study, the measurement of the magnetic field was carried out in 14 lines with a maximum length of 1200 m of measurement path with 10 m and 100 m spacing between measurement stations. The most important thing that must be done before data acquisition is synchronization of geomagnetic devices between devices on the base and mobile such as uniform day, date, month, year, frequency and time of data recording. This is done for the accuracy of the field data and to facilitate data processing. In the data collection process, the thing to note is that the sensor on the tool must face the North-South of the earth because the earth's magnetic pole is in the geographic North-South direction of the earth. Data acquisition was carried out by measuring the magnetic field at measurement stations in each track. At each station, magnetic field measurements were performed 5 times. This is done in order to obtain valid and accurate data. At the same time, daily variation measurements were also carried out at the base station.

Data Processing

Data from the results of magnetic field measurements in the field need to be corrected to obtain total magnetic anomaly data. The corrections made are as follows Daily Correction and IGRF correction. For the daily correction or diurnal correction is the deviation of the value of the earth's magnetic field due to the difference in time and the effects of radiation originating from the sun in one day (Michelsen et al., 2015; Purnomo et al., 2016). This correction is done to eliminate the influence of the external magnetic field or daily variations. In making this daily correction, the corrected time must be in accordance with the measurement time of magnetic field data at each location point (measurement station) (Maryanto, 2017). Daily correction is carried out by adding the daily variation value recorded at a certain time to the magnetic field data to be corrected. This applies if the daily variation is negative. On the other hand, if the daily variation is positive, the correction is made by subtracting the daily variation recorded at a certain time from the magnetic field data to be corrected.

Basically, the results of the measurement of the magnetic field on the earth's surface come from three components, namely the main magnetic field of the earth, the external magnetic field and the anomalous field. The main magnetic field value is the IGRF value. The IGRF value is the largest value that is also measured when measuring with the magnetic method, so corrections are needed to eliminate it. IGRF correction aims to eliminate variations in the magnetic field originating from within the earth. The IGRF value of the study area can be seen on the IGRF calculator by inputting the date data, coordinates of the base station point, as shown in **Figure 3**. The results of the IGRF calculator are the inclination, declination and total magnetic field values (Oskooi & Abedi, 2015; Pirttijärvi et al., 2015).

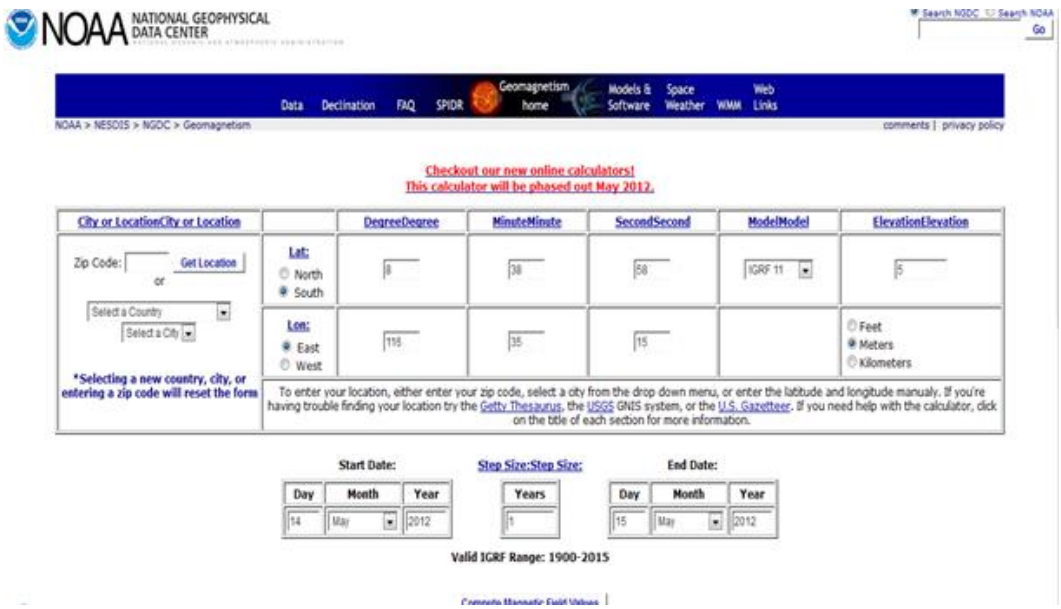

Figure 3. IGRF data input (Source : http://www.ngdc.noaa.gov/geomagmodels/IGRFWMM.jsp)

RESULTS AND DISCUSSION

The magnetic method is a geophysical method that works based on the magnetic properties of rocks found below the earth's surface. This magnetic method measures the value of the total magnetic field anomaly in an area. The magnetic field value obtained is then mapped in the contour of the magnetic field anomaly. Magnetic anomalies provide an overview of the non-uniformity of the Earth's magnetic field (Khalil & Santos, 2014; Mariyanto et al., 2018). This non-uniformity is caused by the distribution of magnetic objects that have different properties and characteristics. Magnetic field anomaly analysis was used to interpret the susceptibility of subsurface geological structures prominent in the study area based on modeling made with the help of Mag2DC software.

Data Processing Results

Magnetic field data obtained in the field is processed using Surfer 9 Software, Numeri Software, Mag2DC Software and MS Office Excel 2013 Software so as to produce magnetic field anomalies. The magnetic field anomaly produced are total magnetic anomaly, regional magnetic anomaly and residual magnetic anomaly in the study area. The three magnetic anomalies from the processing are then interpreted both qualitatively and quantitatively. Meanwhile, the description of the surface conditions of the research area is carried out by collecting data in the form of latitude, longitude and elevation values of the research area.

Daily Correction Results

The following graph shows the results of the daily correction of the magnetic field during field measurements on July 21, 2020. Based on the graph in **Figure 4**, it can be seen that the change in the value of the magnetic field with time during data recording is not very significant. This illustrates that, during the recording of the magnetic field, there is no significant jump in the magnetic field change or there is no magnetic storm. It is said that a magnetic storm occurs when the recorded change in the magnetic field reaches 1,000 nT (Maryanto, 2017).

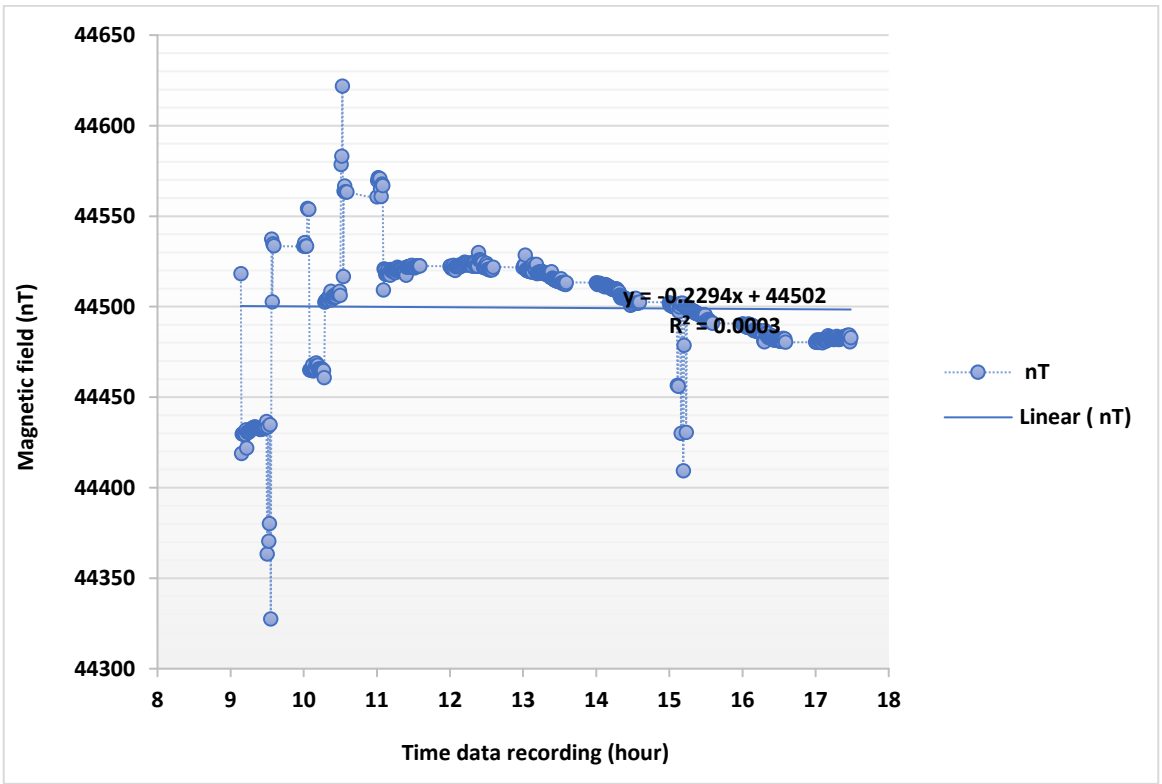

Figure 4. Daily correction

IGRF Correction Results

In this study, the latitude is at coordinates 8° 35' 24" South Latitude and longitude is at coordinates 116° 8' 13" East Longitude with an elevation of 27.6 meters **(Figure 5)**.

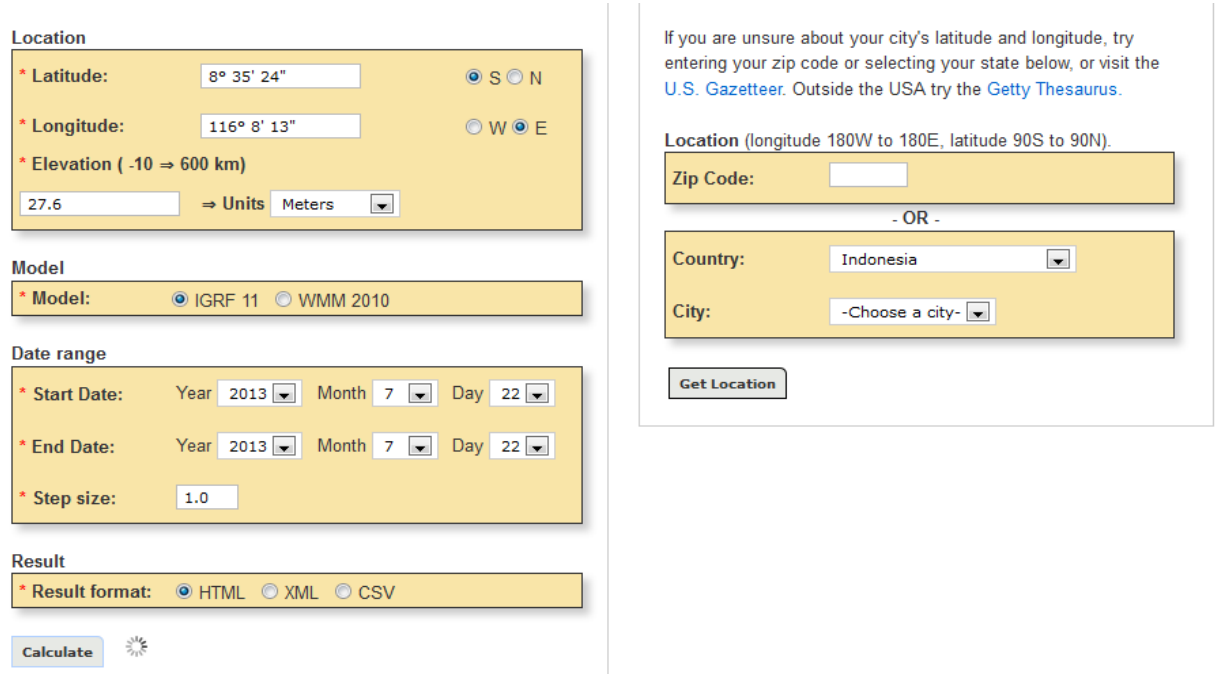

Figure 5. Data input fields on the IGRF Calculator
[Source : http://www.ngdc.noaa.gov/geomagmodels/IGRFWMM.jsp]

The coordinate column determines the latitude and longitude values. Then input the coordinate values (in the form of degrees, minutes and seconds) (Khalil & Santos, 2014; Mariyanto et al., 2018). In the "model" column, "IGRF 11" is selected, while in the "elevation" column the elevation value and units used are input. In the "start date" and "end date" fields, input the start and end time of the measurement (day, month, and year). In the column "step size" input "1". Based on the data that has been entered, the output is obtained in the form of the total magnetic field value as the IGRF value as well as the inclination and declination of the research location as shown in **Table 1**.

Table 1. Output column on IGRF calculator

Date	Declination (+ E | - W)	Inclination (+ D | - U)	Horizontal Intensity	North Comp (+ N | - S)	East Comp (+ E | - W)	Vertical Comp (+ D | - U)	Total Field
2013-07-21	1◦29'16"	-33◦ 50' 59"	37389.3 nT	37376.7 nT	970.8 nT	-25076.9 nT	45020.1 nT
Change/year	-1.7'	5.0'	10.3 nT	10.8 nT	-18.4 nT	71.7 nT	-31.3 nT

Sources : http://www.ngdc.noaa.gov/geomagmodels/IGRFWMM.jsp

Topographic Contour Map

Topography is a description of the shape of the surface of an area on the earth's surface. Topographic contour maps were made with the help of Surfer software version 9. The data entered was in the form of longitude, latitude and elevation data of the research area that had been grounded beforehand (Khalil & Santos, 2014; Mariyanto et al., 2018). The following is a topographic map of Medana Village, Tanjung District, North Lombok Regency, West Nusa Tenggara Province, Indonesia **(Figure 6)**. Based on the 3D topography in **Figure 6**, it is clearer that the research area is in the form of a valley centered in the middle with northeast and northwest directions and in the form of hills in the southwest and north.

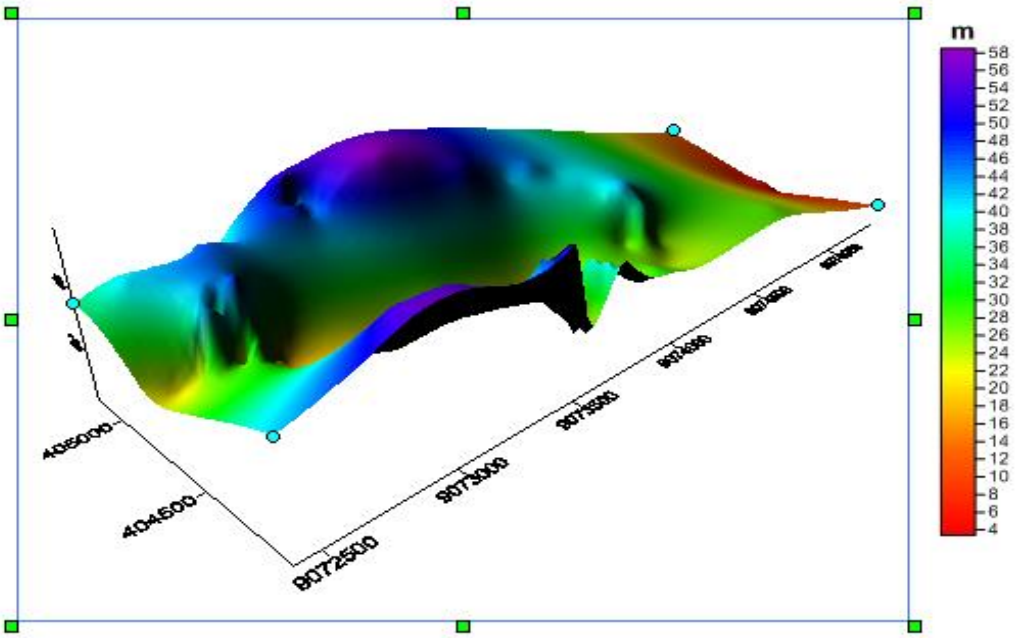

Figure 6. 3D Topographic map of research area

Total Magnetic Anomaly

The total magnetic field anomaly is the value of the magnetic field at a point generated by the rock below the surface that is the target of the magnetic method measurement. The contour of the total magnetic field anomaly is a general description of the subsurface geological conditions, because this anomaly originates from shallow and deep sources of anomaly. The total magnetic field anomaly is generated by reducing the data measured in the field. The reductions carried out are daily variation correction and IGRF correction.

The results of the contouring of the total magnetic field anomaly of the study area can be seen in **Figure 7**, on the contour map it can be seen that the anomaly value ranges from -950 to 150 nT for this study area. The total magnetic field anomaly contour pattern consists of a positive contour color spectrum and a negative contour color spectrum. This positive and negative contour color spectrum indicates that the magnetic field anomaly is a dipole (Gan et al., 2017; Ibrahim et al., 2019; Nugraha et al., 2019; Whiteley et al., 2021). The large number of magnetic dipoles shows that the total magnetic field anomaly is still strongly influenced by local anomalies, on the contours of the total magnetic anomaly, only a few magnetic dipoles can be seen, this illustrates that the local anomaly slightly affects the total magnetic field anomaly in the study area.

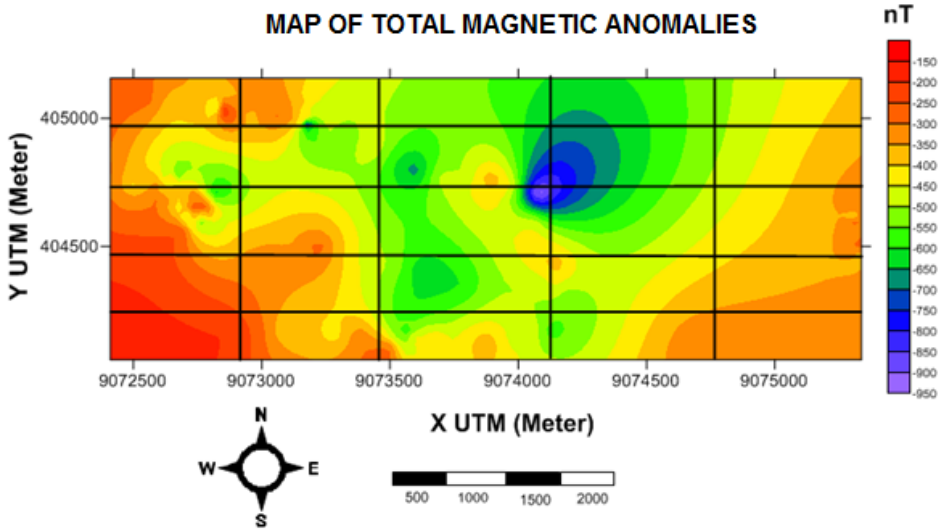

Figure 7. Anomaly map of the total magnetic field of this research area can be grouped into three different anomaly sections, namely low, medium and high anomalies

Regional Anomaly Contour

The regional anomaly contours below are the result of filtering the total magnetic anomaly using the moving average method. In this method, the window width (N) must first be determined. Determination of the width of this window is done by slicing the contour of the magnetic anomaly a total of 8 times. Slicing results data in the form of distances and anomalies are inputted into the Numeri software so that a graph is obtained between the wave number (k) and the natural logarithm of the amplitude (ln A).

Based on the results of the first cross-sectional spectrum analysis in **Figure 8**, it is clear that the difference in slope (gradient) in the two graphs is clearly visible. The gradient value of each of these graphs interprets the depth of the deep source anomaly (regional) and shallow source of the anomaly (residual). Regional anomaly sources are depicted by graphs with a sharper gradient tendency, while shallow anomaly sources are depicted by steeper graph gradients. The results of the first cross-sectional spectrum analysis show that the regional anomaly source has a depth of about 195.52 meters (blue color) and the residual anomaly source has a depth of about 12,353 meters (red color). The average depth of the regional anomaly source is about 201.9913 meters and is interpreted as the base rock of the study area. The average depth of the residual anomaly source field is about 27.75063 meters and is interpreted as a rock layer that is intruded to the surface due to pressure and temperature from within. From the depth of the regional and residual anomalous sources, the thickness of the residual anomaly source can be determined with an average value of about 174.2406 meters.

Table 2. The result of calculating the window width for each section

No	Cross-section	Wave number (k_c)	Value (Δx)	Number (N)
1	Line -AA'	0,0172	29.6	12.25
2	Line -BB'	0,0229	29.6	12.25
3	Line -CC'	0,0229	29.6	12.25
4	Line -DD'	0,023	29.6	9.8
5	Line -EE'	0,0173	29.6	9.25
6	Line -FF'	0,0173	29.6	9.25
7	Line -GG'	0,0173	29.6	9.25
8	Line -HH'	0,022	29.6	12.33
Average		**0,01996**	**29.6**	**10.829**

Sources : Data of this research

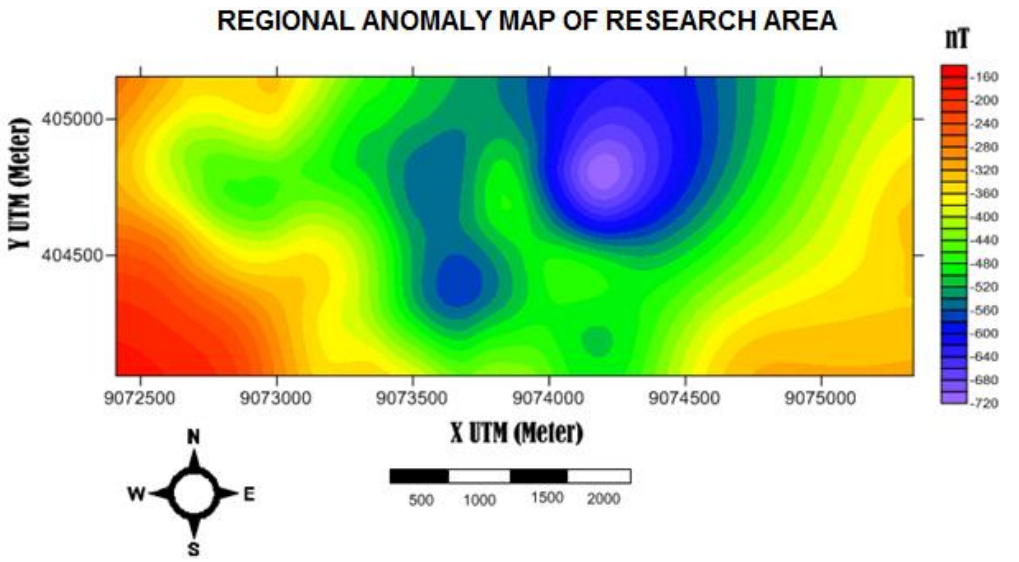

Figure 8. Regional anomaly map

In addition to calculating the depth of field source of regional and residual anomalies, spectrum analysis graphs are also used to determine the window width to be used at the time of filtering. The average value of the k_c cutoff wave number from the eight cross sections of the path is 0.01996, from each k_c cutoff wave number produced, the window width is calculated which will be used as the

window width for filtering the research area. The average window width of the eight sections is 10,829, so the window width used for the filtering process is 11. The window width value for the filtering process is always odd, this is intended to obtain one midpoint as a coordinate plot point. The results of calculating the window width for each section can be seen in **Table 2**.

Based on the results of the filtering of the total magnetic anomaly with a window width of N=11, a regional anomaly contour was obtained **(Figure 8)**. The regional anomaly contour above has a clearer contour pattern when compared to the total magnetic anomaly contour, this is due to the regional anomaly contour the source of the anomaly only comes from the deepest layer which is the basement rock of the investigation area. On the contour of this regional magnetic anomaly, the variation of the anomaly value is between -720 nT to 160 nT. Regional magnetic anomaly values based on the results of this interpretation can be divided into three groups of anomalies, namely high magnetic anomalies, moderate magnetic anomalies and low magnetic anomalies. High magnetic anomaly (red color) is found in the west direction of the study area, medium magnetic anomaly (green-yellow color) is located in the east to west and dominant in the center of the study area and low magnetic anomaly (blue-purple color) is located north to west center of the research area. The research area is dominated by moderate magnetic anomaly. The low magnetic anomaly is in the anomaly value of -720 nT to -560 nT, the moderate magnetic anomaly that dominates the investigation area has a value between -520 nT to -360 nT and the high magnetic anomaly with an anomaly value of -320 nT to -160 nT.

Residual Anomaly Contour

The residual magnetic anomaly is the result of subtracting the total magnetic anomaly with the regional magnetic anomaly resulting from the moving average. The residual magnetic anomaly distribution can be seen in **Figure 9**. The residual magnetic anomaly map shows that the magnetic anomaly distribution is more complex than the regional anomaly because it depicts a magnetic anomaly pattern with a shorter wavelength with a higher frequency which reflects the effect of shallower anomalous objects.

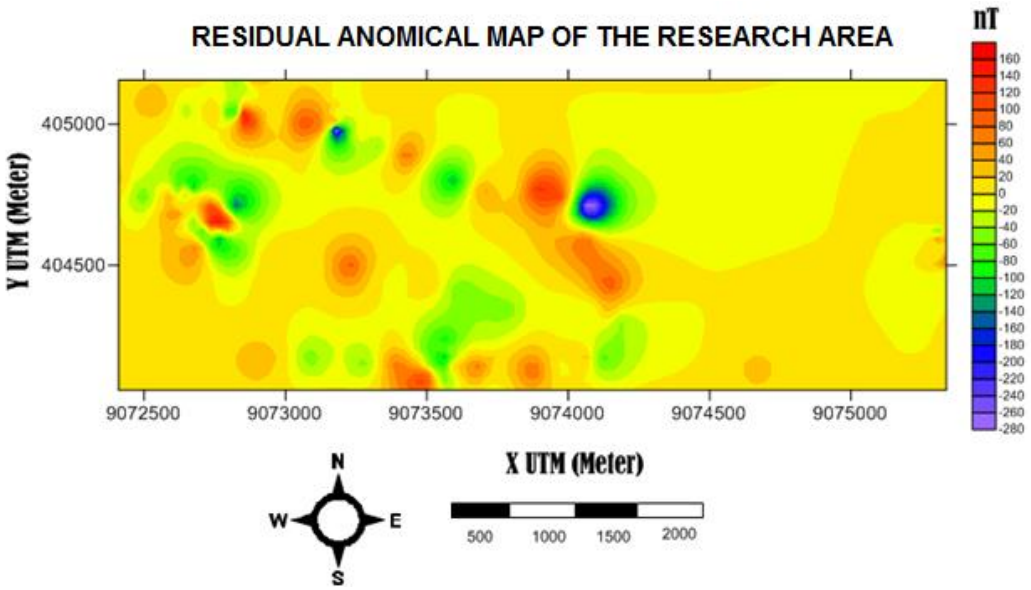

Figure 9. Regional anomaly contour

The residual contour map **(Figure 9)** shows the highest values (red) for residual anomalies of 60 nT to 160 nT appearing slightly in the center of the southwest and north. Moderate anomaly (green-yellow color) with a value of -120 nT with 40 nT spread throughout the study area. Low residual anomalies (purple-blue color) with values of -280 nT to -140 nT are scattered in the center of the study area. Residual anomaly is an anomaly that is the target in determining the condition of the geological structure. The residual anomaly map shows a complex structure, where the contour pattern has a positive anomaly value and a negative anomaly. Positive anomalies are always adjacent to negative anomalies, high positive anomalies are always adjacent to high negative anomalies and

low positive anomalies are always adjacent to low negative anomalies. This shows that the difference in the susceptibility values of rocks below the surface is identified by the presence of faults. By knowing the susceptibility it will be known the type of rock (Gao & Jia, 2020; Orwin, 1998; Thoreau & Prayer, 2000; Zhang et al., 2021).

High magnetic anomaly indicates positive rock susceptibility and high value, and has high magnetic susceptibility. Medium magnetic anomaly indicates a very small negative to positive rock susceptibility and low magnetic anomaly indicates a negative rock susceptibility. It is possible that this low anomaly indicates a weak subsurface geological condition (fault zone) in the area. Residual anomaly is needed in qualitative interpretation, the appearance of the structure that describes the geological conditions below the surface.

Mag2DC inversion modeling

Subsurface conditions are not only adequately explained by qualitative interpretation, therefore quantitative interpretation is necessary to ascertain subsurface conditions based on models and geological conditions of the research area. In this study, quantitative interpretation was carried out by inverse modeling with the aim of matching the anomaly profile with the model profile using Mag2DC software. Inversion modeling is estimating or looking for a model that produces theoretical data that best fits the observation data (rock depth position. The resulting curve pattern indicates the shape or pattern of geological structures, especially faults), so that by matching the observation curve and the calculated curve results will fault structure was obtained at the investigation site (Kusumayudha et al., 2015; Wibberley & Shimamoto, 2003). The modeling of the shape of the faults at each intersection refers to the shape of the anomaly with the fault depiction shown in **Figure 10**.

In this research, there are two paths used for modeling the subsurface structure. Both paths stretch from north to south through negative and positive anomalies. The selection of these two paths is based on anomaly values that can identify the presence of faults in the area. The description of the fault model based on the anomalous graph above **(Figure 10a, Figure 10b and Figure 10c)** is a reference for modeling the fault. A descending fault occurs when there is a fluctuation in the value of the anomaly. On the anomaly contour map, a contour shape will be selected that shows the low-high-low anomaly value. The two paths can be seen in **Figure 11**.

Based on **Figure 11**, the paths AB and CD stretch from north to south through areas with negative anomalies to positive anomalies indicated by dark blue to light yellow for negative anomalies, and dark yellow to orange colors for positive anomalies. This trajectory was chosen with the consideration that the anomaly of the north north central area is very low.

The results of subsurface rock modeling for the AB path obtained five rock layers **(Figure 12)**. The first layer with the model at a depth of 15.8 meters to 31.04 meters with a thickness of 15.16 meters is interpreted as sandstone and gravel with a susceptibility value of 0.031 in Susceptibility (SI) shown in green. The second layer is at a depth of 15.8 meters to 54.9 meters and a thickness of 38.10 meters is interpreted as sandy clay and weathered rock with a susceptibility value of 0.0024 (dala SI) shown in blue. The third layer is at a depth of 51.64 meters to 74.03 meters and a thickness of 22.39 meters is interpreted as limestone with a susceptibility value of 0.0052 (in SI) indicated by dark blue. The fourth layer with the model at a depth of 51.34 meters to 68.96 meters with a thickness of 17.62 meters is interpreted as alluvial rock that has undergone weathering with a susceptibility value of 0.052 (in SI) indicated by the color orange. The fifth layer with the model at a depth of 51.94 meters to 93.13 meters with a thickness of 41.19 meters is interpreted as tuffaceous bresik stone with a susceptibility value of 0.0008 (in SI) indicated by a light blue color.

In this first trajectory, the presence of the fault is thought to be in the third layer with a descending fault type. This descending fault is shown in dark blue, which has a susceptibility value from the anomaly model of 0.0052 (in SI). It is said to be a descending fault because one block fell lower than the base block. The result of the modeling is that there are two fault blocks whose right block is lower or lower than the base block, but has the same susceptibility value (Iwamori, 2007; Tabei et al., 2002; Wibberley & Shimamoto, 2003).

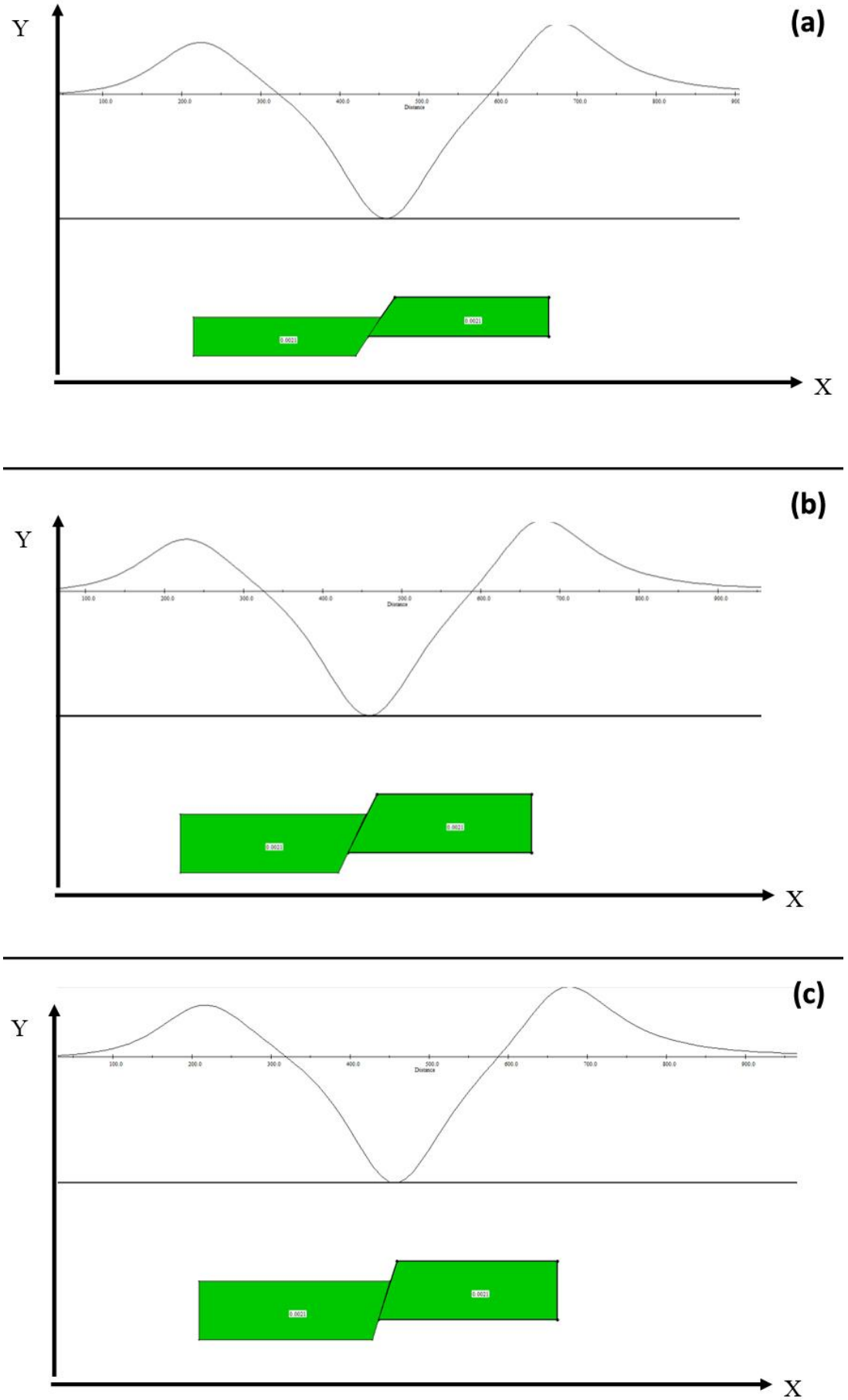

Figure 10. (a) Downward fault with slope angle 30^o, **(b)** Downward fault with slope angle 45^o, **(c)** Downward fault with slope angle 60^o

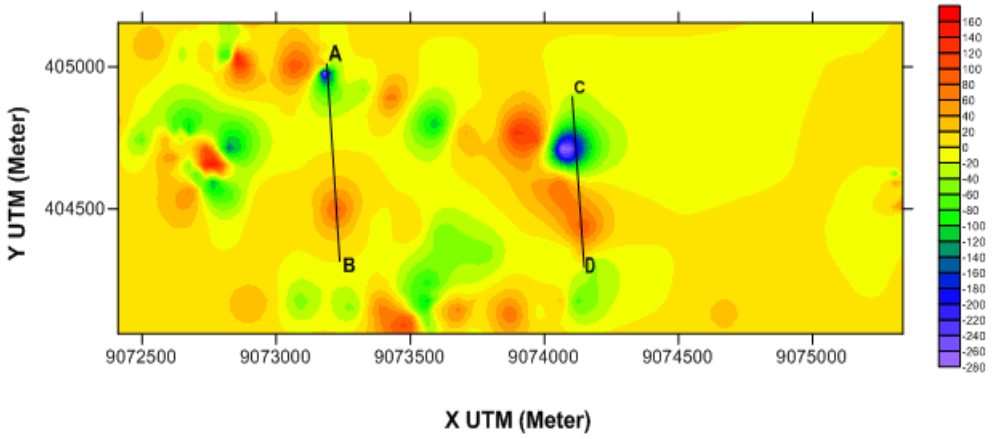

Figure 11. Trajectory on the residual anomaly contour

On the CD path there are four bodies in the cross section of the anomaly model **(Figure 13)**. The first layer with the model at a depth of 15.4 meters to 35.9 meters with a thickness of 19.5 meters is interpreted as gravel sandstone with a susceptibility value of 0.034 (in SI) and minerals that are included in diamagnetic objects with a very small susceptibility value, namely -0.06 (in SI). The second layer is at a depth of 35.8 meters to 42.6 meters and a thickness of 16.8 meters is interpreted as sandy clay and weathered rock with a susceptibility value of 0.00204 (in SI). The third layer is at a depth of 30.4 meters to 57.6 meters and a thickness of 27.5 meters is interpreted as limestone with a susceptibility value of 0.0069 (in SI) indicated by dark blue. The fourth layer with the model at a depth of 44.2 meters to 65.7 meters with a thickness of 21.5 meters is interpreted as tuffaceous bresik rock in the form of sandy clay and gravel with a susceptibility value of 0.0008 (in SI) indicated by blue (Ashok & Umamahesh, 2019; Peker et al., 2024; Weihua et al., 2012). The fifth layer with the model at a depth of 60.6 meters to 87.5 meters with a thickness of 26.9 meters has two types of material, namely alluvial rock that has undergone weathering with susceptibility values (0.0338-0.069) (in SI) indicated by color orange and green and tuffaceous brexic stones with a susceptibility value of 0.0008 (in SI).

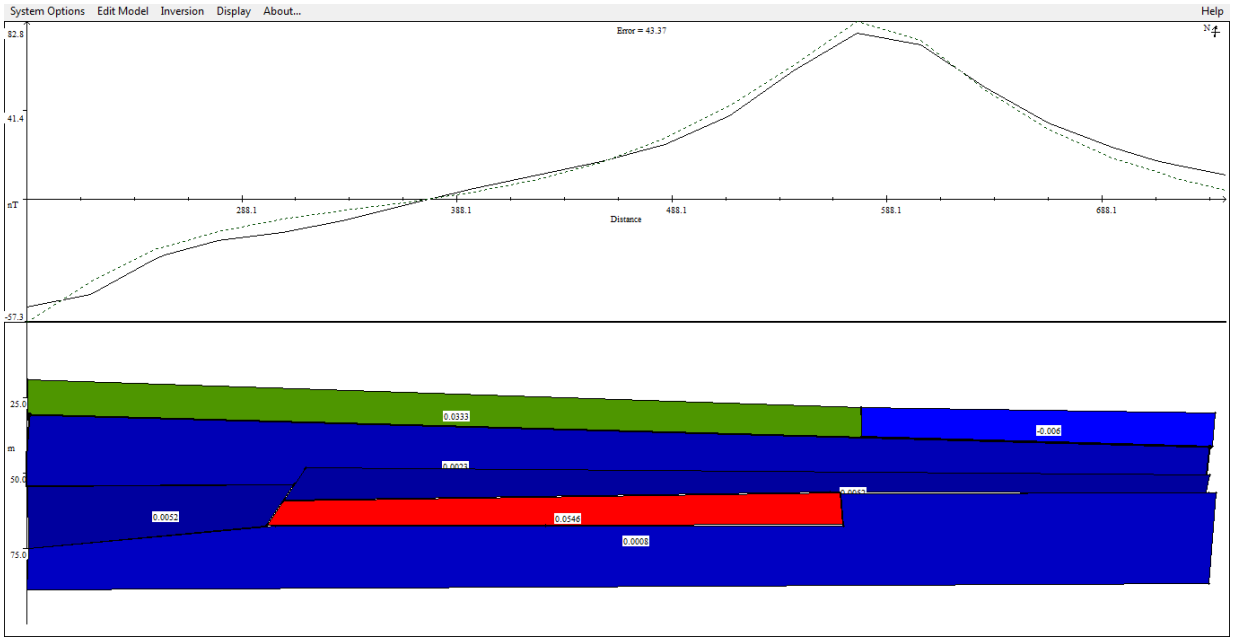

Figure 12. The residual anomaly section of the path AB

In this CD path, the presence of the fault which is the target of the study is thought to be in the third layer which is composed of limestone outcrops with a descending fault type. This descending fault is shown in dark blue, which has a susceptibility value from the anomaly model of 0.00669 (in

SI). It is said to be a descending fault because one block fell lower than the base block. The result of the modeling is that there are two fault blocks whose right block is lower or lower than the base block, but has the same susceptibility value.

The five rocks that cover the surface layer of the study area show low susceptibility values, which range from -0.006 (in SI) to 0.0699 (in SI) and are classified as sedimentary rocks and there are no rocks or minerals that have high susceptibility values such as igneous rocks. Based on the trajectory of the slice from AB to CD which is trending from north to south by passing several positive anomalies and negative anomalies which are blue-orange, it can be indicated that it has decreased and shows the occurrence of a descending fault which has an average susceptibility value of 0.00605 (in SI) with this susceptibility value, the rock type that can be estimated is limestone.

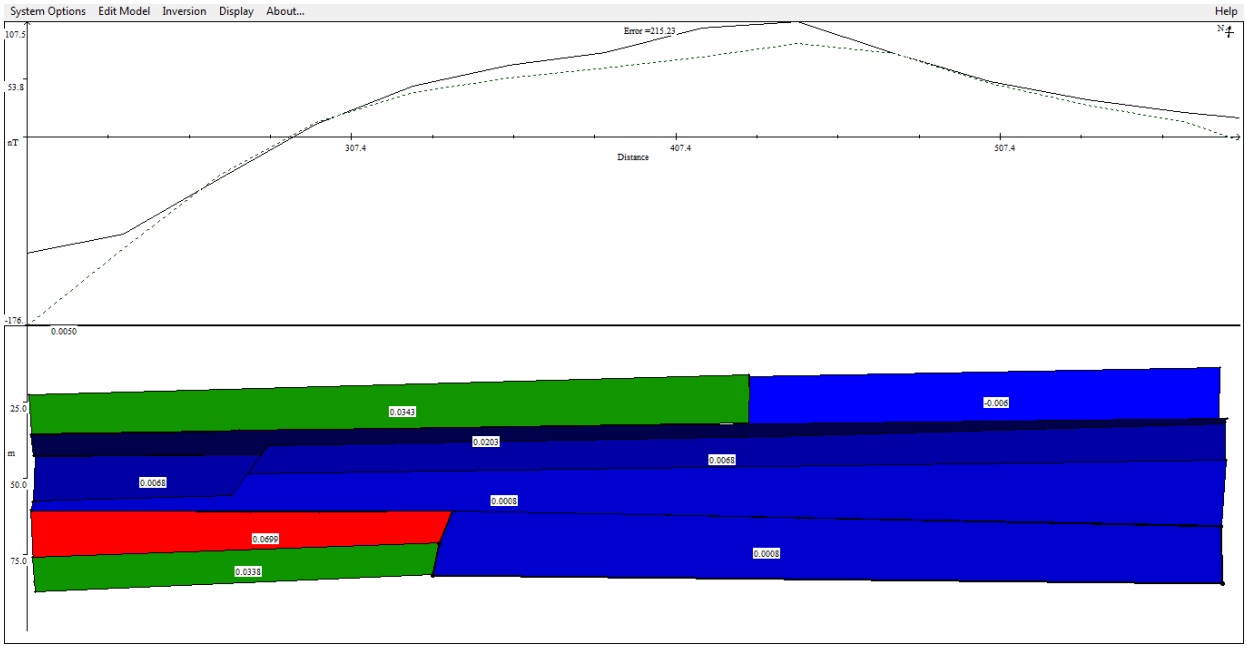

Figure 13. The residual anomaly section of the path CD

Based on the geological map of Lombok Island, the research area is interpreted to be composed of the Qa formation, namely the Alluvial Formation and the coastal deposit. Alluvial Formation is composed of pumice and clay sand, as shown in the geological index of Lombok Island in **Figure 13**. This rock formation is a rock formation originating from coastal deposits and hardened magmatism processes resulting from the Rinjani volcanic deposits with the characteristics of the rocks being easily brittle (Ashok & Umamahesh, 2019; Peker et al., 2024; Weihua et al., 2012). and is hollow, so that if a geological natural disaster occurs, the area with rock characteristics like this is prone to geological disaster damage. This is in accordance with the results of research that has been carried out, where the modeling for the two paths interprets layers with the type of material in the form of sandstone, gravel, clay sand, tuffaceous bresik and alluvial rock that has undergone weathering.

CONCLUSION

Based on the results of data processing, analysis and discussion that has been carried out, it is concluded that modeling the subsurface structure in Orong Ramput Hamlet, Kopang Hamlet and Gol Hamlet, Medana Village, Tanjung District, North Lombok Regency with 2D forward modeling using Mag2DC obtained a subsurface structure that in the form of a normal fault, with an average susceptibility value of 0.00605 (in SI) which is a type of limestone. The depth of this normal fault is estimated to be at a depth of 31.5 meters to 74.0 meters. This research is used as supporting data, so it is necessary to conduct a more thorough study and analysis of the subsurface structure using several supporting methods such as well logging, gravity and geoelectric data.

AUTHOR CONTRIBUTIONS

Conceptualization, HA and VLI; methodology, TS; software, HA; validation, VLI, TS, and HA; formal analysis, VLI; investigation, TS; resources, HA; data curation, VLI; writing—original draft preparation, TS; writing—review and editing, HA; visualization, VLI; supervision, TS; project administration, HA; funding acquisition VLI.

ACKNOWLEDGMENT

The authors are grateful to the anonymous reviewers for their valuable comments and efforts to improve this manuscript.

CONFLICT OF INTERESTS

The authors declare no conflict of interest concerning the publication of this article. The authors also confirm that the data and the article are free of plagiarism.

REFERENCES

Ashok, V., & Umamahesh, R. N. V. (2019). Assessment of inundation risk in urban floods using HEC RAS 2D. *Modeling Earth Systems and Environment*, *5*(4), 1839–1851. https://doi.org/10.1007/s40808-019-00641-8

Diani, R., Herliantari, H., Irwandani, I., Saregar, A., & Umam, R. (2019). Search, Solve, Create, and Share (SSCS) Learning Model: The Impact on the Students' Creative Problem-Solving Ability on the Concept of Substance Pressure. *Jurnal Penelitian Fisika Dan Aplikasinya (JPFA)*, *9*(1), 65. https://doi.org/10.26740/jpfa.v9n1.p65-77

Gan, F., Han, K., Lan, F., Chen, Y., & Zhang, W. (2017). Multi-geophysical approaches to detect karst channels underground — A case study in Mengzi of Yunnan Province, China. *Journal of Applied Geophysics*, *136*, 91–98. https://doi.org/10.1016/j.jappgeo.2016.10.036

Gao, M., & Jia, S. (2020). Primary Investigation on Equivalent Anchoring Method of Jointed Rock Mass Tunnel and Its Engineering Application. *Advances in Civil Engineering*, *2020*. https://doi.org/10.1155/2020/3407875

Haerudin, N., Fitriawan, H., Siska, D., & Farid, M. (2019). Earthquake Disaster Mitigation Mapping By Modeling Of Land Layer And Site Effect Zone. *Jurnal Ilmiah Pendidikan Fisika Al-Biruni*, *08*(1), 53–67. https://doi.org/10.24042/jipfalbiruni.v8i1.3705

Haseeb, M., Bibi, A., Khan, J. Z., Ahmad, I., & Malik, R. (2011). Construction of Earthquake Resistant Buildings and Infrastructure Implementing Seismic Design and Building Code in Northern Pakistan 2005 Earthquake Affected Area. *International Journal of Business and Social Science*, *2*(4), 168–177.

Ibrahim, E., Gultaf, H., Saputra, H., Agustina, L. K., Rahmanda, V., Suhendi, C., Sudibyo, M. R. P., & Rizki, R. (2019). Preliminary Result: Identification of Landslides Using Electrical Resistivity Tomography Case Study Mt. Betung. *Journal of Science and Application Technology*, *2*(1), 107–110. https://doi.org/10.35472/281455

Iwamori, H. (2007). Transportation of H2O beneath the Japan arcs and its implications for global water circulation. *Chemical Geology*, *239*(3–4), 182–198. https://doi.org/10.1016/j.chemgeo.2006.08.011

Khalil, M. A., & Santos, F. M. (2014). On the depth to anomaly estimation using Karous and Hjelt filter in VLF-EM data. *Arabian Journal of Geosciences*, *7*(10), 4355–4359. https://doi.org/10.1007/s12517-013-1110-3

Mahla, M. (2018). *Earthquake resistant structure building*. 1036–1038.

Mariyanto, M., Bahri, A. S., Utama, W., Lestari, W., Silvia, L., Lestyowati, T., Anwar, M. K., Ariffiyanto,

W., Hibatullah, A. I., & Amir, M. F. (2018). Relation Between Transport Distance with Frequency-Dependent Volume Magnetic Susceptibility in Surabaya River Sediments. *Jurnal Penelitian Fisika Dan Aplikasinya (JPFA)*, *8*(1), 33. https://doi.org/10.26740/jpfa.v8n1.p33-41

Maryanto, S. (2017). Geo Techno Park potential at Arjuno-Welirang Volcano hosted geothermal area, Batu, East Java, Indonesia (Multi geophysical approach). *AIP Conference Proceedings*, *1908*(2017). https://doi.org/10.1063/1.5012712

Meijaard, E., Dennis, R. A., Saputra, B. K., Draugelis, G. J., Qadir, M. C. A., & Garnier, S. (2019). Rapid Environmental and Social Assessment of Geothermal Power Development in Conservation Forest of Indonesia. *Proceedings World Geothermal Congress 2020 Reykjavik, Iceland, April 26 – May 2, 2020*, *August*, 1–12.

Michelsen, N., Reshid, M., Siebert, C., Schulz, S., Knöller, K., Weise, S. M., Rausch, R., Al-Saud, M., & Schüth, C. (2015). Isotopic and chemical composition of precipitation in Riyadh, Saudi Arabia. *Chemical Geology*, *413*, 51–62. https://doi.org/10.1016/j.chemgeo.2015.08.001

Nugraha, A. S., Darsono, D., & Legowo, B. (2019). Identification of the distribution of andesite rocks in Kalirejo Village, Kokap District, Kulon Progo Regency, Special Region of Yogyakarta based on geoelectrical tomography data. *Journal of Physics: Conference Series*, *1153*(1). https://doi.org/10.1088/1742-6596/1153/1/012019

Orwin, J. F. (1998). The application and implications of rock weathering-rind dating to a large rock avalanche, Craigieburn Range, Canterbury, New Zealand. *New Zealand Journal of Geology and Geophysics*, *41*(3), 219–223. https://doi.org/10.1080/00288306.1998.9514806

Oskooi, B., & Abedi, M. (2015). Magnetic and electromagnetic data interpretation for delineating geological contacts in the Tomelilla area, Sweden. *Arabian Journal of Geosciences*, *8*(6), 3971–3984. https://doi.org/10.1007/s12517-014-1501-0

Peker, B., Demir, V., Orhan, O., & Beden, N. (2024). Integration of HEC-RAS and HEC-HMS with GIS in Flood Modeling and Flood Hazard Mapping. *Sustainability (Switzerland)*, *16*(3), 1226. https://doi.org/10.3390/su16031226

Pirttijärvi, M., Zaher, M. A., & Korja, T. (2015). Combined inversion of airborne electromagneticand static magnetic field data. *Geophysica*, *50*(2), 65–87. https://doi.org/10.13140/RG.2.1.1747.0486

Purnomo, B. J., Pichler, T., & You, C. F. (2016). Boron isotope variations in geothermal systems on Java, Indonesia. *Journal of Volcanology and Geothermal Research*, *311*, 1–8. https://doi.org/10.1016/j.jvolgeores.2015.12.014

Sari Bahagiarti Kusumayudha, Jatmiko Setiawan, Ayu N. Ciptahening, & Prabawa Dwi Septianta. (2015). Geomorphologic Model of Gunungsewu Karst, Gunung Kidul Regency, Yogyakarta Special Territory, Indonesia: The Role of Lithologic Variation and Geologic Structure. *Journal of Geological Resource and Engineering*, *4*(1), 1–7. https://doi.org/10.17265/2328-2193/2015.01.001

Sherpa, D. (2010). *Earthquake Resistant Building Construction*. *Civil*, 11.

Tabei, T., Hashimoto, M., Miyazaki, S., Hirahara, K., Kimata, F., Matsushima, T., Tanaka, T., Eguchi, Y., Takaya, T., Hoso, Y., Ohya, F., & Kato, T. (2002). Subsurface structure and faulting of the Median Tectonic Line, southwest Japan inferred from GPS velocity field. *Earth, Planets and Space*, *54*(11), 1065–1070. https://doi.org/10.1186/BF03353303

Taruna, R. M., & Banyunegoro, V. H. (2018). Earthquake Relocation Using Double Difference Method for 2D Modelling of Subducting Slab and Back Arc Thrust in West Nusa Tenggara. *Jurnal Penelitian Fisika Dan Aplikasinya (JPFA)*, *8*(2), 132. https://doi.org/10.26740/jpfa.v8n2.p132-143

Thoreau, H. D. (2010). *Plate Tectonics* (pp. 1–32).

Thoreau, H. D., & Prayer, Y. I. (2000). *Rocks & Minerals* (p. 38).

Watlet, A., Van Camp, M., Francis, O., Poulain, A., Rochez, G., Hallet, V., Quinif, Y., & Kaufmann, O. (2020). Gravity Monitoring of Underground Flash Flood Events to Study Their Impact on Groundwater Recharge and the Distribution of Karst Voids. *Water Resources Research*, *56*(4), 1–18. https://doi.org/10.1029/2019WR026673

Weihua, W., Zhijun, L., Jing, L., Yan, H., & Zengping, C. (2012). *Procedia Engineering A Real-time Target Detection Algorithm for Panorama Infrared Search and Track System*. *29*, 1201–1207. https://doi.org/10.1016/j.proeng.2012.01.113

Wekke, I. S., Sabara, Z., Samad, M. A., Yani, A., & Umam, R. (2019). Earthquake , Tsunami , And Society Cooperation : Early Findings In Palu Post Of Indonesia Disaster. *INA-Rxiv Papers*. https://doi.org/10.31227/osf.io/xmcyn

Whiteley, J. S., Watlet, A., Uhlemann, S., Wilkinson, P., Boyd, J. P., Jordan, C., Kendall, J. M., & Chambers, J. E. (2021). Rapid characterisation of landslide heterogeneity using unsupervised classification of electrical resistivity and seismic refraction surveys. *Engineering Geology*, *290*(May), 106189. https://doi.org/10.1016/j.enggeo.2021.106189

Wibberley, C. A. J., & Shimamoto, T. (2003). Internal structure and permeability of major strike-slip fault zones. *Journal of Structural Geology*, *25*, 59–78.

Zhang, S., Gao, R., Meng, Q., & Zhang, X. (2021). Research on Rock Resistant Coefficient in Lining Tunnels Based on the Generalized Hoek-Brown Failure Criterion. *Geofluids*, *2021*(1968). https://doi.org/10.1155/2021/5554644